ACS OMEGA

Article

Cite This: ACS Omega 2017, 2, 7976-7984

http://pubs.acs.org/journal/acsodf

Effect of Platinum, Gold, and Potassium Additives on the Surface Chemistry of CdI_2-Antitype Mo_2C

Merve Demirtas,[†] Hande Ustunel,[†,*] and Daniele Toffoli[‡,*]

[†]Department of Physics, Middle East Technical University, Dumlupinar Bulvari 1, 06800 Ankara, Turkey

[‡]Dipartimento di Scienze Chimiche e Farmaceutiche, Università degli Studi di Trieste, Via L. Giorgieri 1, I-34127 Trieste, Italy

ABSTRACT: Transition metal carbides are versatile materials for diverse industrial applications including catalysis, where their relatively low cost is very attractive. In this work, we present a rather extensive density functional theory study on the energetics of adsorption of a selection of atomic and molecular species on two Mo terminations of the CdI_2 antitype phase of Mo_2C. Moreover, the coadsorption of CO in the presence of preadsorbed metal atoms and its dissociative adsorption in the absence and presence of preadsorbed Pt and K were investigated. By using CO as a probe to understand the structural/electronic effects of the preadsorption of the metal atoms on the $Mo_2C(001)$ surface, we showed that K further enhances CO adsorption/activation on the surface, in contrast to the precious metals considered. Moreover, it was observed that the presence of both Pt and K stabilizes the transition state for the C−O bond dissociation, lowering the activation barrier for the dissociation of the C−O bond by about 0.3 and 0.4 eV, respectively.

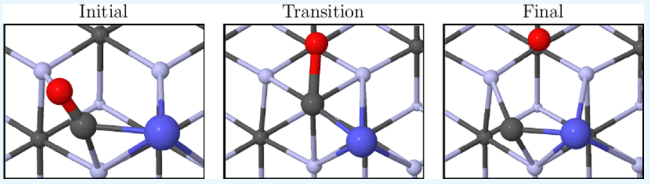

1. INTRODUCTION

Transition metal carbides (TMCs) have attracted considerable attention in diverse industrial applications since the early 1970s due to their superior materials properties including extreme hardness,[1] high melting point,[2] high electrical/thermal conductivity,[3] and superconductivity.[4] Recently, their value as high-performance catalysts has also been recognized. They have been used in many industrially important processes such as hydrodenitrogenation,[5] CO hydrogenation,[6] and hydrodesulfurization.[7] In particular, several reports have highlighted the higher activity and durability of TMCs in the context of the water−gas-shift (WGS) reaction when compared to the commercial Cu−Zn catalysts.[8−10]

One of the promising TMCs, proposed recently as a catalyst for the WGS reaction is Mo_2C.[11] Mo_2C can be characterized by several crystal structures, with different relative stabilities depending on the temperature.[12] In the orthorhombic structure, the Mo atoms are organized on a hexagonal sublattice with C atoms occupying half of the octahedral sites in an orderly manner. In the hexagonal phase, the Mo atoms exhibit a hexagonal close packing, with the C atoms statistically occupying half of the octahedral sites. The hexagonal phase can further be classified as eclipsed or CdI_2 antitype, depending on the arrangement of the carbon atoms.[13] As both hexagonal and orthorhombic phases are constructed based on a hexagonal Mo network, these phases are interchangeably referred to as either α or β in the literature, causing some confusion in the nomenclature adopted by different authors.[14−16] To circumvent this confusion, we adopted the explicit naming convention CdI_2 antitype, recently used by Tominaga et al.[17] and Wang et al.[18] for referring to the polymorph studied in the present work.

Considerable effort has been channeled toward studying the adsorption of molecules on several Mo_2C surfaces. Detailed density functional theory (DFT) investigations of atomic and molecular adsorption of small species such as H, O, CO, and NO, important for various reactions, have been conducted on various clean Mo_2C surfaces.[19−21] Adsorption of most of these species proceed through either the formation of strong covalent bonds or Coulombic interactions, both accompanied by a large charge transfer. Furthermore, the effect of promoters such as K[13] and Rb[14] and coadsorption of the reactant and intermediate species participating in the reactions have also been explored.[18]

In addition to the energetics of adsorption, computational data on activation barriers, relevant for the WGS and other reactions, are also available. In a DFT study, Tominaga and Nagai calculated the reaction barriers of all of the intermediate steps involved in the redox mechanism of the WGS reaction on a clean, CdI_2 antitype-$Mo_2C(001)$ surface.[22] The rate-determining step was identified as the reaction between the adsorbed CO and O to produce CO_2. Several possible CO and NO dissociation pathways were explored by Shi et al. in a cluster DFT study, and a wide range of activation energies were identified depending on the initial conditions.[19] The elementary steps of the syngas reaction on several Mo_xC_y stoichiometries were studied by Medford et al., and their activity was found to be larger than that of metal catalysts.[23] Activation of CO_2 and H_2 in the context of methanol synthesis,[24] CO dissociation,[18,21] CO hydrogenation,[25] and

Received: July 21, 2017
Accepted: November 3, 2017
Published: November 15, 2017

DOI: 10.1021/acsomega.7b01044
ACS Omega 2017, 2, 7976−7984

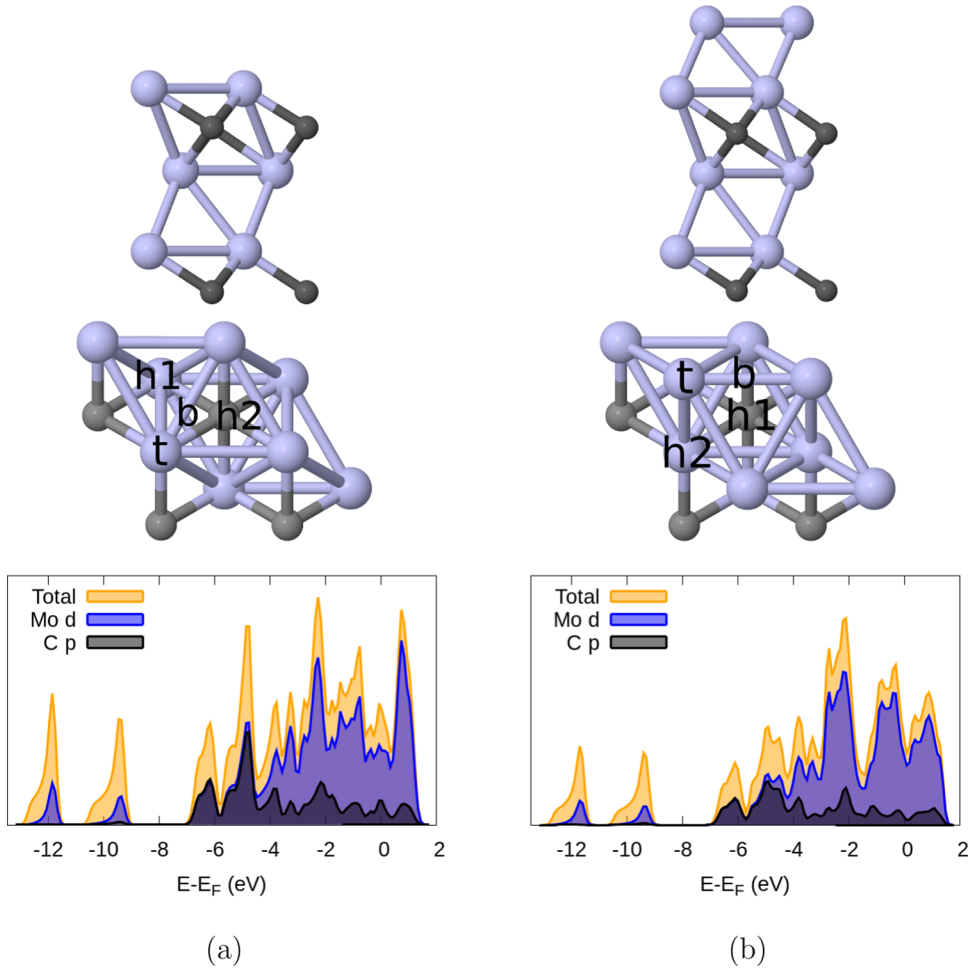

Figure 1. Side view (upper panels) and top view (middle panels) of the 2 × 2 surface slabs of the two Mo terminations of the $Mo_2C(001)$ surface, Mo1 (a) and Mo2 (b). The labeling scheme of different adsorption sites and the projected density of states (PDOS's) are also reported in the middle and lower panels, respectively.

hydrogen production from formic acid[26] are further recent examples.

The interaction of metals and Mo_2C is of great interest in the catalysis community.[27−30] Mo_2C has been successfully used as a heterogeneous catalyst in several reactions including toluene hydrogenation,[31,32] hydrodeoxygenation of acetone[33] and methyl stearate,[34] hydrogen evolution reaction,[35] ethanol dissociation,[36] and CO generation.[37] In addition to bare Mo_2C, several examples of Mo_2C-based catalysts, enhanced with a small amount of Pt-group metals such as Pt, Ir, Pd; precious metals such as Ag and Au or other transition metals such as Ni and Cu have been screened for activity and selectivity in a large number of experiments.[28,38−45] The results reported in these works reveal that whereas some of the metals have no effect on the activity of the Mo_2C substrate, others induce a significant increase. Many of these studies also indicate that the activity of the supported metal depends sensitively upon many parameters, such as the amount of interfacial strain, the morphologies of the Mo_2C support and metal component, the loading, and the temperature. In light of these results, an atomistic-scale study of the surface chemistry of Mo_2C by itself and when enriched with metals is necessary.

In the present work, we explore, via ab initio gradient-corrected density functional theory, the surface chemistry of the two Mo terminations of the $Mo_2C(001)$ surface in the absence and presence of an alkali promoter (K) and two precious metals (Au and Pt). We tackle this problem in three stages. First, we present calculated adsorption energies of several atomic (H, O, C, Pt, Au, and K) and molecular (H_2O, CO, and CO_2) species relevant to many important heterogeneous reactions. We then explore the effect of preadsorbed Pt, Au, and K on the energetics of adsorption of CO, which is used as a probe molecule to sample the electronic and structural effects induced by the preadsorbed atomic species. Finally, we calculate the activation energies of a simple yet important reaction, namely CO dissociation in the absence and in the presence of a single preadsorbed Pt and K atom. Preliminary calculations suggest that the activation energy of CO dissociation on the $Mo_2C(0001)$ surface is not affected by the presence of a preadsorbed Au atom. CO dissociation is a key step in various important reactions such as CO hydrogenation.[21]

We would like to stress that although there have been extensive reports on the adsorption characteristics of CO on the surfaces of both orthorhombic and eclipsed hexagonal phase and other small molecules such as NO,[19] a complete account of the adsorption properties of all of the adsorbates considered in this work on the CdI_2-antitype phase is absent from the literature. As far as the promoters and precious metals are concerned, only K[13,14,16,46] has been explored somewhat extensively on Mo_2C surfaces. In the very few studies involving

DOI: 10.1021/acsomega.7b01044
ACS Omega 2017, 2, 7976−7984

the CdI_2-antitype phase, only one Mo termination has been considered. The present work aims to give a more complete account of the adsorption and reaction characteristics of both terminations and a wider range of molecules, promoters, and coverages.

The article is organized as follows. In Section 2, we detail our computational method. In Section 3, we present and discuss our results, whereas our conclusions are presented in Section 4.

2. COMPUTATIONAL DETAILS

The calculations presented in this work were performed within the plane-wave pseudopotential DFT framework.[47,48] The Perdew−Wang (PW91) exchange correlation functional[49] as implemented in Quantum Espresso[50] was employed in all of the calculations. The open-source programs XCrysDen[51] and JMol[52] were used for visualization and to produce the figures. During Broyden−Fletcher−Goldfarb−Shanno geometry optimizations, a force threshold per atom of approximately 0.001 eV/Å was used. The use of ultrasoft pseudopotentials[53] to model the interaction between atomic nuclei and electrons allowed an affordable kinetic energy cutoff of 40 Ryd and a density cutoff of 400 Ryd.

The CdI_2-antitype phase of Mo_2C has a hexagonal structure with a unit cell of 3 atoms, and an experimental c/a ratio of 1.58[54] ($a = b = 3.01$ Å and $c = 4.77$ Å). In the present work, the lattice constants were calculated using two methods: a fixed-volume calculation with the experimental volume and the variable-cell method of Wentzcovitch,[55] which optimizes the cell shape along with the electronic and nuclear degrees of freedom. The fixed-volume calculations yielded 1.7 and −3.4% errors with respect to the experimental a and c, respectively, whereas the errors for the variable-cell method are 3.0 and −2.1%. In the remaining calculations, we use the fixed-volume values. These results are in reasonable agreement with previous theoretical studies.[14,18]

The CdI_2-antitype phase Mo_2C has an ABCABC... repeating pattern of nonstoichiometric layers along the (0001) direction. Two consecutive Mo layers are followed by a C layer, giving rise to two Mo-terminated and one C-terminated surfaces. In this work, the two Mo-terminated (0001) surfaces were modeled using a 2 × 2 slab with five or six layers. Whereas the five-layer slab corresponds to a Mo termination with a C subsurface layer, the six-layer slab has two Mo layers on the top. In all of our slab calculations, the atomic coordinates of the two bottommost layers were fixed to their value in the bulk to mimic bulk behavior. In a study by Shi et al.,[19] the Mo_2C substrate was represented by a cluster model and the CO adsorption energy was reported to only differ by about 0.1 eV even for modest cluster sizes. This is confirmed by our slab model study (vide infra).

In all of the calculations, a vacuum layer of at least 14 Å was used to minimize the interaction between periodic images. A Monkhorst−Pack grid[56] of 8 × 8 × 1 points was used to perform the Brillouin zone integrations for the 2 × 2 slab and scaled back accordingly with increasing cell size in other calculations. The geometry-optimized surfaces, shown in Figure 1, will be referred to as Mo1 and Mo2 in the following. The calculated Mo1−C, C−Mo2, and Mo2−Mo1 bulk interlayer distances are 1.17, 1.17, and 2.34 Å, respectively. During geometry optimization, the surfaces do not undergo any significant reconstruction or appreciable deviation of the interlayer distances with respect to the bulk values. The partial density of states (PDOS's) are also shown in Figure 1, where the block of states around the Fermi level (at the zero of the energy axis) are contributed by Mo d and C p orbitals. The two surface terminations do not display appreciable differences in their PDOS profiles, in line with the lack of extensive reconstruction.

Atomic and molecular adsorption energies were calculated at various adsorption sites in a 2 × 2 surface cell. The adsorption energy, E_b, is calculated according to

$$E_b = E_{Mo_2C+ads} - E_{Mo_2C} - E_{ads} \quad (1)$$

where E_{Mo_2C+ads} is the total energy of the Mo_2C surface and the adsorbate, E_{Mo_2C} is the total energy of the clean surface, and E_{ads} is the energy of the adsorbate. With this definition, stable adsorption geometries have negative adsorption energy. Atomic adsorption energies (i.e., for H, O, C, Pt, Au, and K) were referenced to the single atom in the gas phase. Vibrational frequencies of the adsorbed species were also calculated, and no imaginary frequencies were found. A large cubic simulation cell (with a side length of 30 Å) was employed for the calculations of isolated atoms and molecules, and the relevant total energy calculations were conducted using the same cutoff energy values as the bulk and surface calculations, but at the Γ point of the Brillioun zone.

The effect of the preadsorbed precious metal atoms (Pt and Au) and the promoter (K) on the energetics of CO adsorption was investigated by calculating the adsorption energy of CO on a surface with a single preadsorbed metal atom (Pt, Au, or K). The CO adsorption energy is therefore calculated as

$$E_b(X+CO) = E_{Mo_2C+X+CO} - E_{Mo_2C+X} - E_{CO} \quad (2)$$

where X represents a preadsorbed Pt, Au, and K species. $E_b(X + CO)$ can directly be compared to E_b for CO calculated according to eq 1. To quantify the effect of preadsorption, we use the energy difference

$$\Delta E_b = E_b(CO) - E_b(X + CO) \quad (3)$$

With the definition of eq 3, a positive ΔE_b indicates an increase in the stability of the adsorbate in the presence of the preadsorbed metal atom.

The climbing image nudged elastic band (CI-NEB) method was employed[57] for the calculation of the activation barrier for the dissociation of CO(CO → C + O). The optimization of the initial and final states was carried out before the NEB calculation, and conducted in a 2 × 3 slab only on the Mo1-terminated surface. Following the identification of the reactant and product configurations, the optimization of the reaction path was conducted over seven images. Spin polarization was not included in the NEB calculations.

As the charge transfer upon adsorption is an important parameter describing the adsorbate−surface interaction, the partial charges on the atomic or molecular adsorbates were calculated by using the Bader decomposition, as implemented by the Henkelman group.[58]

3. RESULTS AND DISCUSSION

3.1. Energetics of Atomic and Molecular Adsorption on the Mo-Terminated Mo_2C(0001) Surfaces. For the atomic and molecular adsorption calculations, four initial, high-symmetry sites were chosen, as indicated in Figure 1. On both Mo-terminated surfaces (Mo1 and Mo2), two distinct threefold (hexagonal) sites were considered: h1 and h2. In the case of the Mo1 termination, the h1 site has a Mo atom underneath in the

DOI: 10.1021/acsomega.7b01044
ACS Omega 2017, 2, 7976−7984

Table 1. Adsorption Energies (E_b, in eV) and Bader Charges (q, in |e|) of Atomic Adsorbates on the Two Mo Surface Terminations

	O		H		C		Pt		Au		K	
site	E_b	q	E_b	q	E_b	q	E_b	q	E_b	q	E_b	q
Mo1 h1	−6.52	−1.2	−3.16	−0.6	−7.12	−1.6	−5.76	−0.9	−3.75	−0.6	−2.18	0.70
Mo1 h2	−6.71	−1.2	−3.02	−0.6	−6.89	−1.6	−5.85	−0.9	−3.80	−0.6	−2.16	0.70
Mo1 t	−5.41	−1.0	−2.63	−0.5	−4.74	−0.9	−4.55	−0.8	−3.04	−0.5	−2.12	0.70
Mo1 b	h1	−1.3	h1	−0.6	h1	−1.6	h2	−0.9	h2	−0.6	−2.16	0.70
Mo2 h1	−7.61	−1.3	−3.46	−0.7	−8.37	−1.7	−6.67	−1.1	−4.32	−0.8	−2.05	0.69
Mo2 h2	−7.85	−1.3	−3.34	−0.7	−8.22	−1.7	−6.53	−1.0	−3.99	−0.8	−2.04	0.69
Mo2 t	−6.09	−1.0	−2.11	−0.5	−5.04	−0.9	−6.85	−1.1	−4.39	−0.8	−2.00	0.69
Mo2 b	−7.79	−1.2	h2	−0.6	h2	−1.7	h2	−1.1	h2	−0.8	−2.05	0.69

third layer, whereas h2 is directly above the second-layer C atom. For the Mo2 termination, h1 has a C atom underneath in the third layer, whereas h2 has a Mo atom in the second layer. The remaining high-symmetry sites are the on-top (t) and the twofold bridge (b) positions. All of the adsorbates were placed at a distance of approximately 2 Å above the surface sites and subjected to geometry optimization. The adsorption energies and charges on the adsorbates for the atomic and molecular species are reported in Tables 1 and 2, respectively. In several

Table 2. Adsorption Energies (E_b, in eV) and Bader Charges (q, in |e|) of Molecular Adsorbates on the Two Mo Surface Terminations

	CO		CO_2		H_2O	
site	E_b	q	E_b	q	E_b	q
Mo1 h1	−1.86	−0.10	b	−1.06	t	−0.07
Mo1 h2	−1.50	−0.86	b	−1.06	−0.16	−0.06
Mo1 t	−2.11	−0.57	−1.77[a]		−0.81	−0.07
Mo1 b	−2.00	−0.77	−1.12	−1.06	−0.46	−0.11
Mo2 h1	−2.54	−1.13	−1.86	−1.20	t	−0.05
Mo2 h2	−2.32	−1.12	b	−1.19	t	−0.07
Mo2 t	−1.90	−0.53	b	−1.19	−0.80	−0.06
Mo2 b	h1	−1.13	−1.85	−1.20	−0.84	−0.11

[a]Dissociative adsorption energy.

instances, during geometry optimization, the initial adsorbate configuration relaxed to a different high-symmetry site. When different from the initial adsorption site, the final location is indicated, along with the computed E_b value in the tables. In particular, many of the species considered moved away from the initial bridge site. Occasionally, the adsorbate was observed to depart from the high-symmetry configurations shown and either tilt slightly with respect to the surface in the case of molecules or move to a location that cannot be clearly labeled as h1, h2, or t. Both the tilting of the molecules and the migration toward a more stable adsorption site are consistent with previous observations from the literature.[19]

Atomic and molecular adsorptions are characterized by a large charge transfer from the surface to the adsorbate. The observed electron donation properties of the $Mo_2C(0001)$ surfaces agrees with past investigations.[19,24] Overall, for O, C, and H atomic species, the surface-to-adsorbate charge transfer is similar for both Mo terminations. On the other hand, for Pt, Au, and CO, the surface with the Mo2 termination donates a somewhat larger amount of charge upon adsorption than the Mo1 termination. This difference is particularly pronounced for CO adsorption on the h1 site. For adsorbed K, the charge donation is from the adsorbate to the surface; this chemically intuitive result is in accord with the works of Pistonesi et al.,[13,46] both in terms of direction of the charge transfer and its magnitude.

The adsorption energies and the charge transfers calculated for the atomic species reveal a strong adsorbate−surface interaction. For all of the adsorption sites considered, Pt, Au, C, and O adsorbates show a stronger affinity for the Mo2 surface. This is also the case for H adsorption on the more stable h1 and h2 sites, whereas the energetics of K adsorption is less sensitive to the two different surface terminations and the adsorption site. For the Mo1 termination, h1 and h2 are the most stable adsorption sites for all of the atomic species considered. In the case of the Mo2 termination, the situation is less clear-cut. However metal adatoms behave somewhat differently in the sense that the t site becomes the preferred adsorption site for Au and Pt, at variance with C, O, and H. It is clear that differences in the structural and electronic properties of the two Mo terminations substantially affect the interaction with metallic and nonmetallic adatoms.

CO preferentially adsorbs in the C-down configuration. The computed E_b value for CO adsorption in the O-down configuration is very small at all of the sites, about −0.15 eV for the on-top configurations for both Mo1 and Mo2 terminations, and less than −0.03 eV for all of the other configurations, in agreement with the work of Shi et al.[19] The C−O bond length for CO adsorbed on the Mo1 surface varies between 1.16 and 1.19 Å, depending on the adsorption site, whereas it is larger on the Mo2 surface, with a value of about 1.21 Å (except for the t adsorption site, for which R(C−O) = 1.16 Å). These bond lengths are slightly larger than the calculated gas phase value of 1.14 Å and indicate a weakening and activation of the C−O bond upon adsorption. The larger C−O bond length of the adsorbed CO on the Mo2 termination compared to that relative to Mo1 parallels the increased amount of charge transfer to the adsorbate on the Mo2 termination. On the Mo1 surface, CO remains on the initial adsorption site after geometry optimization, the only exception being the b site, where the CO molecule tilts during geometry optimization by 59° with respect to the surface plane. On the Mo2 surface, on the other hand, a CO molecule, initially placed on the b site, is observed to migrate toward the hollow h1 site. Overall, we see that different terminations of the same surface stabilize different adsorption sites; on the Mo1 termination, CO binds preferentially at bridge and on-top sites, on the other hand, hollow sites h1 and h2 are seen to be the preferred adsorption sites on the Mo2 termination.

Triatomic molecules exhibit a more complex adsorption behavior, with alterations in the bond angles in addition to the bond lengths with respect to their gas phase values. The CO_2

DOI: 10.1021/acsomega.7b01044
ACS Omega 2017, 2, 7976−7984

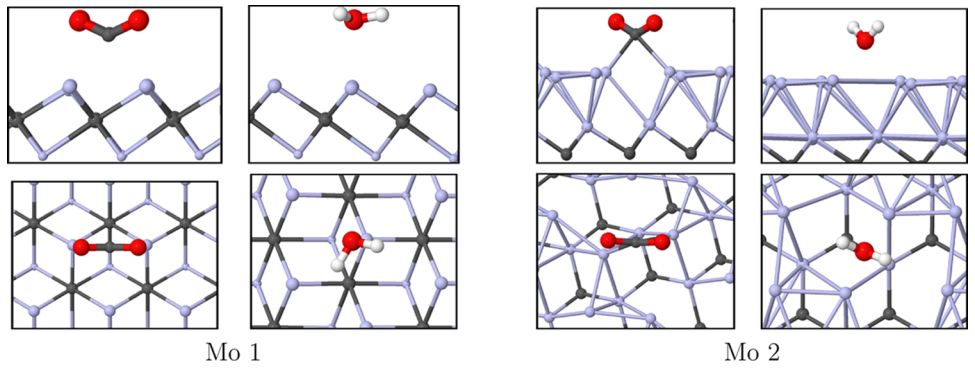

Figure 2. Most stable adsorption modes for CO_2 (bridge on Mo1 and Mo2) and H_2O (on-top on Mo1 and bridge on Mo2) on the two Mo-terminated surfaces. Upper panels display the side view, whereas the lower panels display the top view of the geometries.

molecule, which is linear in the gas phase, bends with a O−C−O angle of about 135 and 131° for the Mo1 and Mo2 terminations, respectively. This is consistent with the charge transfer from the surfaces to CO_2. In contrast, H_2O hardly acquires any charge from the surface, in line with the larger equilibrium distance from the surface, with vertical O-surface distances ranging from 2.31 to 3.26 Å. The H−O−H angles are calculated to be in the range 104−112°. The computed value of E_b, although much smaller than the value corresponding to CO_2, is still relatively high and close to −1.0 eV. The H_2O molecule also causes a mild rearrangement of the surface Mo atoms on both Mo-terminated surfaces. From the data collected in Table 2, we conclude that H_2O preferentially adsorbs at the t and b sites. Its placement at the h1 and h2 sites results in either a migration to the t site or, in the case of Mo1 h2, a small adsorption energy. These results qualitatively agree with the results of a recent work[59] on H_2O adsorption on the metallic (001) surface of the eclipsed hexagonal phase. CO_2, on the other hand, was found to adsorb dissociatively on the Mo1 termination, when it was initially placed on the t site. From the results reported in Table 2, we then conclude that the molecular adsorption of CO_2 is stabilized on the b site for both surface terminations. The adsorption geometry, involving two Mo−O interactions and with the C atom pointing downward, is shown in Figure 2. Overall, the geometries of molecularly adsorbed CO_2 are in reasonable agreement with an earlier theoretical study of Ren et al.[60] on the Mo-terminated orthorhombic phase.

To characterize the effect of the preadsorption of the alkali promoter and the noble metals, we investigate their coadsorption with CO. The choice of CO as a suitable probe molecule is due to its importance in many industrially relevant reactions.[19] In each calculation, Pt, Au, and K were preadsorbed on the h2, h2, and h1 sites, respectively, as these were the most stable adsorption sites for the single species on the Mo1 surface, and the CO probe was placed on the neighboring h1, h2, t-Mo, and t-X (X = Pt, Au, or K) sites. Here, we distinguish between t-Mo and t-X, as the former is the site where the adsorbate is placed on top of a nearby surface Mo atom, whereas the latter refers to a configuration where the adsorbate is directly on top of the precious metal or the promoter. All of the adsorbates placed on the h1 and h2 sites migrated to the t-Mo site upon geometry relaxation, so that the presence of the preadsorbed metal atom does not change the relative stability of CO adsorption sites on the Mo1 surface. We accordingly only consider the t-Mo and the t-X adsorption sites in the following discussion. To check the convergence of the quoted numbers against surface coverage, the coadsorption calculations were repeated in 2 × 3, 3 × 2, and 3 × 3 surface slabs. The adsorption energies calculated for all of the four coverages studied vary by at most 0.05 eV, which indicates the reliability of our results even at the smallest coverage. The optimized adsorption geometries are shown in Figure 3, and the adsorption energies are given in Table 3.

Several conclusions can be drawn from the analysis of the results reported in Table 3. Interestingly, the presence of the noble metals does not substantially affect the stability of the coadsorbed CO on the t-Mo site, despite the electron-withdrawing effect that the preadsorbed Au and Pt have on

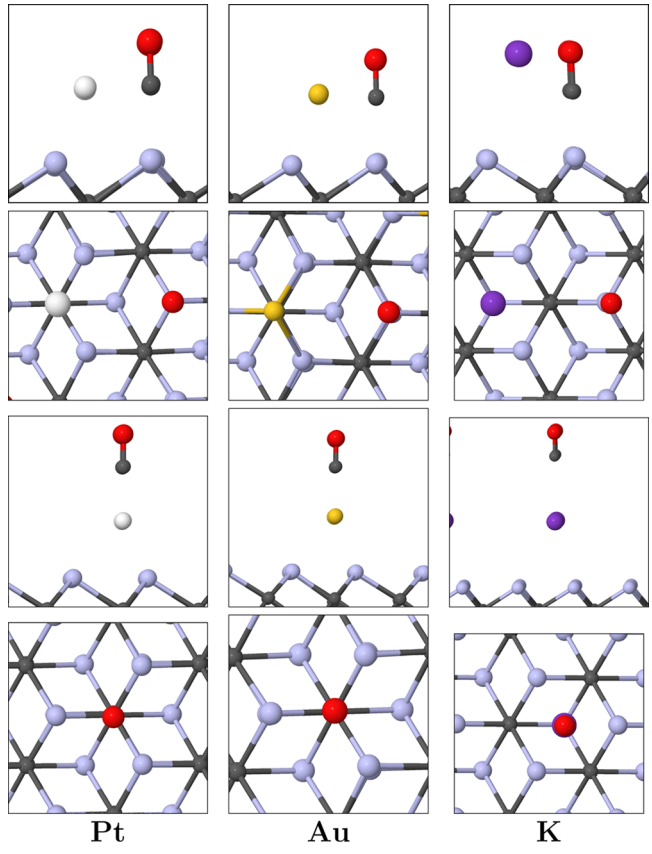

Figure 3. CO adsorption with coadsorbed Pt (left panels), Au (middle panels), and K (right panels) atoms on the Mo1-terminated surface. The top two panels show the t-Mo configurations, whereas the bottom two show the t-X configurations.

DOI: 10.1021/acsomega.7b01044
ACS Omega 2017, 2, 7976−7984

Table 3. CO Adsorption Energies on Promoted Surfaces (E_b(X + CO), in (eV))[a]

sites	E_b(X + CO)	E_b(CO)	ΔE_b	q_{CO}	q_M	d(CO)
Pt h2/CO t-Mo	−2.05	−2.11	−0.07	−0.50	−0.83	1.16
Au h2/CO t-Mo	−2.06	−2.11	−0.07	−0.09	−0.43	1.17
K h1/CO t-Mo	−2.37	−2.11	0.25	−0.92	+0.81	1.20
Pt h2/CO t-Pt	−1.87			−0.15	−0.69	1.16
Au h2/CO t-Au	−0.50			−0.55	−0.52	1.15
K h1/CO t-K	−2.39			−0.09	+0.74	1.14

[a]The variation in the adsorption energy due to the coadsorbed metal atom is also indicated (see text for details), together with the C−O bond length (Å) and the Bader charge on the adsorbate and the metal atom, q_M (|e|).

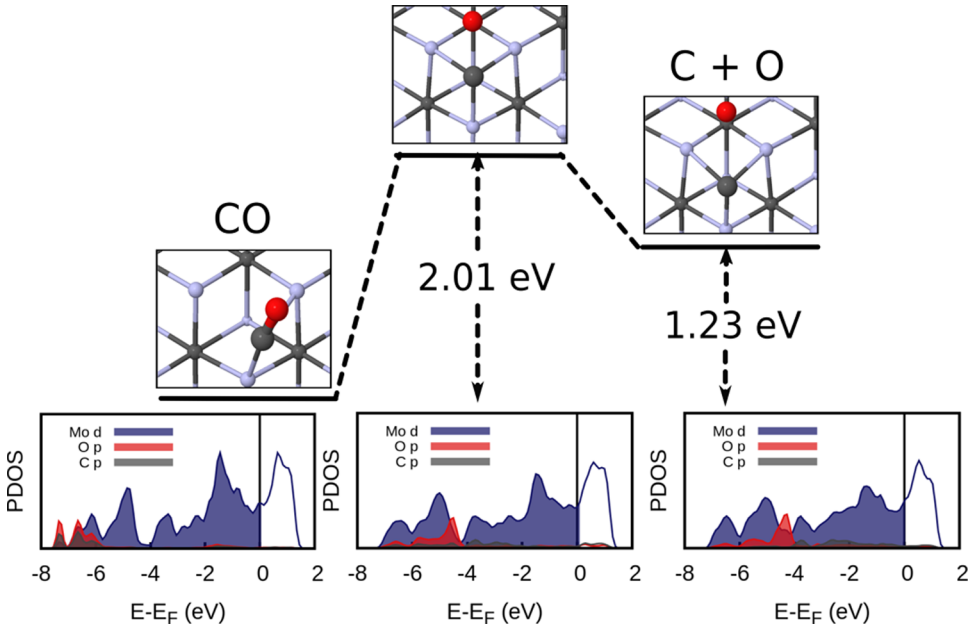

Figure 4. CO dissociation profile on the clean $Mo_2C(001)$ surface along with the projected density of states (bottom panels).

the Mo1 surface and discussed above. The presence of preadsorbed K further stabilizes and activates CO, and this can be understood as a surface-mediated electron donation from K to CO. A similar result was observed in the DFT study by Pistonesi et al. on the β-polymorph of Mo_2C.[46] It is also interesting to note that a similar adsorption energy for CO on t-M is obtained when M = K, whereas a lower adsorption energy (and a lower activation of the CO molecule) is observed for the t-Pt and t-Au configurations. It would be interesting to see if these trends are conserved also for the preadsorbed Au and Pt clusters and how the presence of the metal cluster modulates the CO activation compared to the pristine surface and to other TMC-supported metal clusters.[24]

3.2. CO Dissociative Adsorption on the $Mo_2C(0001)$ Surface. It is interesting at this point to assess the effects of preadsorbed metal and alkali atoms on the activation barrier of a simple reaction on the $Mo_2C(0001)$ surface, namely, CO dissociation. Here, we concentrate only on the Mo1 surface. Transition metal carbides are thought to be active catalysts for a variety of important chemical reactions without the need for noble metals such as Pt or Au. This aspect is important for the development of active catalysts at a reduced cost.

The dissociation of the CO molecule, starting from a tilted on-top geometry, as shown in Figure 4, is characterized by an activation barrier of 2.01 eV on the clean surface, in good agreement with a very recent study on CO dissociation on the CdI_2-antitype Mo-terminated (001) surface.[18] In the transition state, the CO molecule sits almost parallel to the surface, with a C−O bond length of 1.80 Å. In the final state, C and O atoms are located on the neighboring hollow sites. For the same reaction, in the presence of Pt, shown in Figure 5, the calculated barrier is lower with a value of 1.74 eV. The active participation of the Pt atom in the scission of the C−O bond is both visually evident from the geometry of the transition state, reported in Figure 5 and reflected in the PDOS data presented in the same figure. The peaks between −2 and −4 eV in the initial configuration in the presence of Pt indicate a Pt d−C p hybridization. The effects in the bond distances in the initial state are more subtle; the C−O bond lengths are 1.21 and 1.23 Å without and with the Pt atom, respectively. At the same time, in the transition state, C is observed to lose a total of 0.2 |e| of electrons with respect to the transition state in the absence of Pt. The C−O bond length in the transition state, in contrast, is around 1.8 Å for both systems with and without Pt. We see overall that Pt lowers the activation energy by stabilizing the transition state.

An interesting observation is that the presence of Pt lowers the reaction energy of CO dissociation by about 0.5 eV by means of stabilizing the final state, as seen in the reaction profiles in Figures 4 and 5. This is due mostly to the direct bond created between the C and the Pt atoms with a bond length of 2.0 Å, which is very close to the nearest-neighbor Pt−C distance in zincblende PtC.[61] In addition, the difference in the PDOS profiles of the final configurations presented in

DOI: 10.1021/acsomega.7b01044
ACS Omega 2017, 2, 7976−7984

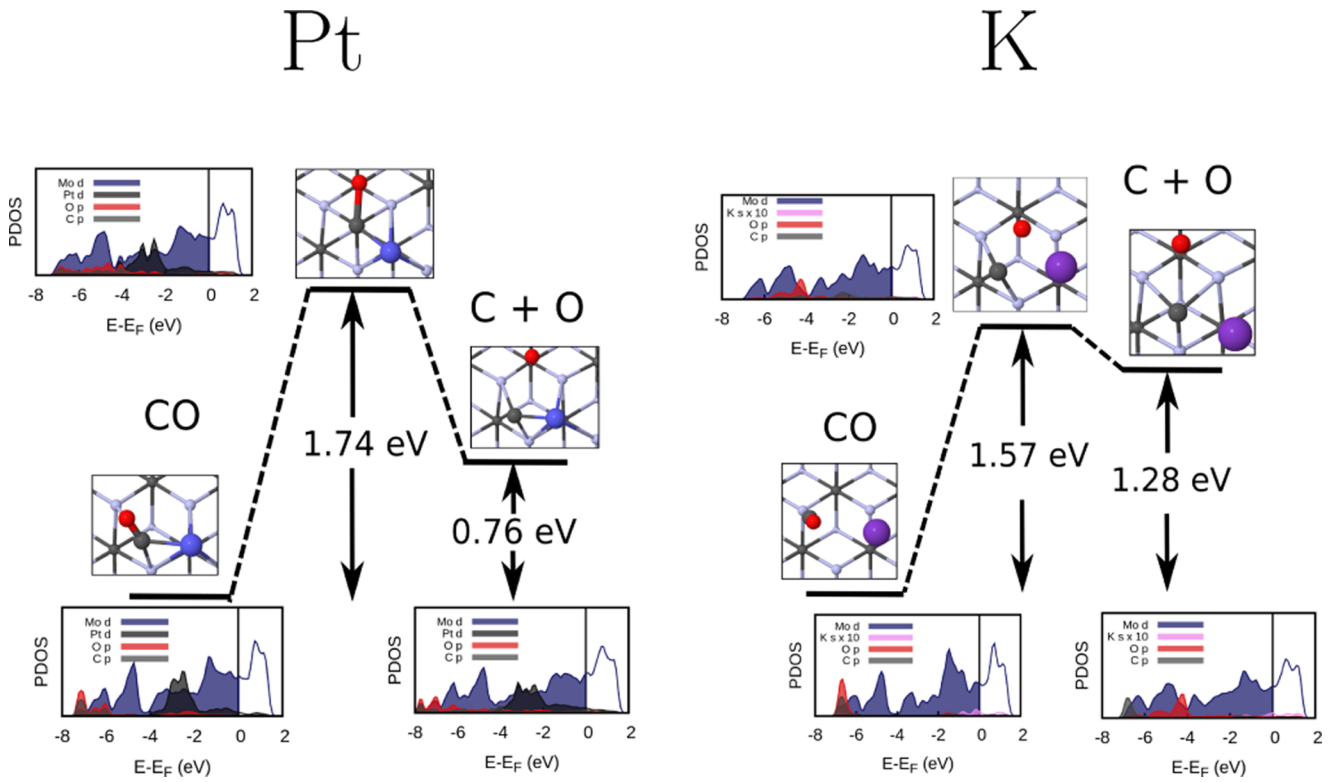

Figure 5. CO dissociation profiles on the Pt- and K-promoted $Mo_2C(001)$ surface along with the projected density of states of the initial, transition, and final configurations.

Figures 4 and 5 (left panel) is evident. The C p states appear at much lower energies and express overlap with the Pt d states.

In the presence of coadsorbed K, the reaction barrier reduces to 1.57 eV (Figure 5, right panel), 0.44 eV lower in comparison to the bare surface and 0.17 eV lower in comparison to the Pt-promoted surface. This can be attributed to a greater stabilization of the transition state in the presence of K compared to both the bare surface and in the presence of coadsorbed Pt. Similar to the Pt adsorbate, the K atom participates directly in the C−O bond dissociation, but by interacting with both atomic fragments of the CO molecule. In the transition state, the C−K and O−K distances are 2.97 and 2.63 Å, whereas the elongated C−O bond (1.91 Å) is longer than the value (1.8 Å) characteristic of the transition state on both the bare surface and in the presence of Pt. This also means that the geometry of the transition state resembles more closely that corresponding to the final state, which accounts also for the larger value of reaction energy computed in the presence of the K promoter compared to Pt. This last point is also evident from the strict similarity of the PDOS profiles corresponding to the transition state and final state reported in the right panel of Figure 5.

4. CONCLUSIONS

The adsorption energies of several atomic (H, O, C, Pt, Au, and K) and molecular (CO, H_2O, and CO_2) species on two Mo terminations of the CdI_2-antitype phase of Mo_2C were calculated in the density functional theory framework. Moreover, the coadsorption of CO in the presence of preadsorbed metal atoms and the dissociative adsorption of CO in the absence and presence of preadsorbed Pt and K were also investigated to provide a detailed understanding of the surface chemistry of the hexagonal Mo_2C that can be used as a starting point for a complete characterization of this TMC for processes relevant in catalysis.

The Mo_2C substrate acts as electron donor for all of the atomic and molecular species considered, with the exception of the alkaline metal. In particular, the effect of the TMC is to activate both CO and CO_2, as revealed from the lengthening of the C−O bond and the bending of the CO_2 molecule upon adsorption. Moreover, by using CO as a probe to understand the structural/electronic effects of the preadsorption of the metal atoms on the $Mo_2C(001)$ surface, we showed that K further enhances CO adsorption/activation on the surface, in contrast with the precious metals considered.

Finally, the dissociative CO adsorption was investigated both in the absence and in the presence of preadsorbed Pt and K. It was observed that the presence of the Pt and K stabilizes the transition state, lowering the activation barrier for the dissociation of the C−O bond by about 0.3 and 0.44 eV, respectively.

AUTHOR INFORMATION

Corresponding Authors

*E-mail: ustunel@metu.edu.tr (H.U.).
*E-mail: toffoli@units.it (D.T.).

ORCID

Hande Ustunel: 0000-0003-0307-9036
Daniele Toffoli: 0000-0002-8225-6119

Notes

The authors declare no competing financial interest.

ACKNOWLEDGMENTS

This work is financially supported by TÜBITAK, Scientific and Technological Research Council of Turkey (Grant No.

DOI: 10.1021/acsomega.7b01044
ACS Omega 2017, 2, 7976−7984

112T542). D.T. also acknowledges partial funding from the project "Small molecules: keys for sustainable development" (Finanziamento per Ricerca di Ateneo 2016-2017) of the University of Trieste, Italy.

REFERENCES

(1) Liao, J.; Wilcox, R.; Zee, R. Structures and properties of the Mo-Mo_2C system. *Scr. Metall. Mater.* **1990**, *24*, 1647−1652.
(2) Hwu, H. H.; Chen, J. G. Surface chemistry of transition metal carbides. *Chem. Rev.* **2005**, *105*, 185−212.
(3) Nelson, J. A.; Wagner, M. J. High surface area nanoparticulate transition metal carbides prepared by alkalide reduction. *Chem. Mater.* **2002**, *14*, 4460−4463.
(4) Xu, C.; Wang, L.; Liu, Z.; Chen, L.; Guo, J.; Kang, N.; Ma, X.-L.; Cheng, H.-M.; Ren, W. Large-area high-quality 2D ultrathin Mo_2C superconducting crystals. *Nat. Mater.* **2015**, *14*, 1135−1142.
(5) Schwartz, V.; da Silva, V. T.; Oyama, S. T. Push-pull mechanism of hydrodenitrogenation over carbide and sulfide catalysts. *J. Mol. Catal. A: Chem.* **2000**, *163*, 251−268.
(6) Park, K. Y.; Seo, W. K.; Lee, J. S. Selective synthesis of light olefins from syngas over potassium-promoted molybdenum carbide catalysts. *Catal. Lett.* **1991**, *11*, 349−356.
(7) Rodriguez, J. A.; Dvorak, J.; Jirsak, T. Chemistry of thiophene on Mo(110), MoC_x and MoS_x surfaces: photoemission studies. *Surf. Sci.* **2000**, *457*, L413−L420.
(8) Moon, D. J.; Ryu, J. W. Molybdenum carbide water-gas shift catalyst for fuel cell-powered vehicles applications. *Catal. Lett.* **2004**, *92*, 17−24.
(9) Levy, R. B.; Boudart, M. Platinum-like behavior of tungsten carbide in surface catalysis. *Science* **1973**, *181*, 547−549.
(10) Asara, G. G.; Roldan, A.; Ricart, J. M.; Rodriguez, J. A.; Illas, F.; de Leeuw, N. H. New insights into the structure of the C-terminated β-Mo₂C (001) surface from first-principles calculations. *J. Phys. Chem. C* **2014**, *118*, 19224−19231.
(11) Patt, J.; Moon, D. J.; Phillips, C.; Thompson, L. Molybdenum carbide catalysts for water-gas shift. *Catal. Lett.* **2000**, *65*, 193−195.
(12) dos Santos Politi, J. R.; Vines, F.; Rodriguez, J. A.; Illas, F. Atomic and electronic structure of molybdenum carbide phases: bulk and low Miller-index surfaces. *Phys. Chem. Chem. Phys.* **2013**, *15*, 12617−12625.
(13) Pistonesi, C.; Juan, A.; Farkas, A.; Solymosi, F. Effects of potassium on the adsorption of methanol on β-Mo 2 C (001) surface. *Surf. Sci.* **2010**, *604*, 914−919.
(14) Han, J. W.; Li, L.; Sholl, D. S. Density functional theory study of H and CO adsorption on alkali-promoted Mo_2C surfaces. *J. Phys. Chem. C* **2011**, *115*, 6870−6876.
(15) Wang, T.; Liu, X.; Wang, S.; Huo, C.; Li, Y.-W.; Wang, J.; Jiao, H. Stability of β-Mo_2C Facets from ab Initio Atomistic Thermodynamics. *J. Phys. Chem. C* **2011**, *115*, 22360−22368.
(16) Pronsato, M.; Pistonesi, C.; Juan, A.; Farkas, A.; Bugyi, L.; Solymosi, F. Density Functional Theory Study of Methyl Iodide Adsorption and Dissociation on Clean and K-Promoted β-Mo_2C Surfaces. *J. Phys. Chem. C* **2011**, *115*, 2798−2804.
(17) Tominaga, H.; Aoki, Y.; Nagai, M. Hydrogenation of CO on molybdenum and cobalt molybdenum carbides. *Appl. Catal., A* **2012**, *423−424*, 192−204.
(18) Wang, T.; Tian, X.; Yang, Y.; Li, Y.-W.; Wang, J.; Beller, M.; Jiao, H. Coverage dependent adsorption and co-adsorption of CO and H_2 on the CdI_2-antitype metallic Mo_2C(001) surface. *Phys. Chem. Chem. Phys.* **2015**, *17*, 1907−1917.
(19) Shi, X.-R.; Wang, J.; Hermann, K. CO and NO Adsorption and Dissociation at the β-Mo_2C (0001) Surface: A Density Functional Theory Study. *J. Phys. Chem. C* **2010**, *114*, 13630−13641.
(20) Ren, J.; Huo, C.-F.; Wang, J.; Li, Y.-W.; Jiao, H. Surface structure and energetics of oxygen and CO adsorption on α-Mo 2 C (0001). *Surf. Sci.* **2005**, *596*, 212−221.
(21) Wang, T.; Li, Y.-W.; Wang, J.; Beller, M.; Jiao, H. High Coverage CO Adsorption and Dissociation on the Orthorhombic Mo_2C(100) Surface. *J. Phys. Chem. C* **2014**, *118*, 3162−3171.
(22) Tominaga, H.; Nagai, M. Density functional theory of water-gas shift reaction on molybdenum carbide. *J. Phys. Chem. B* **2005**, *109*, 20415−20423.
(23) Medford, A. J.; Vojvodic, A.; Studt, F.; Abild-Pedersen, F.; Norskov, J. K. Elementary steps of syngas reactions on Mo 2C(0 0 1): Adsorption thermochemistry and bond dissociation. *J. Catal.* **2012**, *290*, 108−117.
(24) Posada-Pérez, S.; Viñes, F.; Rodriguez, J. A.; Illas, F. Fundamentals of Methanol Synthesis on Metal Carbide Based Catalysts: Activation of CO_2 and H_2. *Top. Catal.* **2015**, *58*, 159−173.
(25) Qi, K. Z.; Wang, G. C.; Zheng, W. J. A first-principles study of CO hydrogenation into methane on molybdenum carbides catalysts. *Surf. Sci.* **2013**, *614*, 53−63.
(26) Luo, Q.; Wang, T.; Walther, G.; Beller, M.; Jiao, H. Molybdenum carbide catalysed hydrogen production from formic acid - A density functional theory study. *J. Power Sources* **2014**, *246*, 548−555.
(27) Ma, Y.; Guan, G.; Hao, X.; Zuo, Z.; Huang, W.; Phanthong, P.; Li, X.; Kusakabe, K.; Abudula, A. Embedded structure catalyst: a new perspective from noble metal supported on molybdenum carbide. *RSC Adv.* **2015**, *5*, 15002−15005.
(28) Sabnis, K. D.; Cui, Y.; Akatay, M. C.; Shekhar, M.; Lee, W. S.; Miller, J. T.; Delgass, W. N.; Ribeiro, F. H. Water-gas shift catalysis over transition metals supported on molybdenum carbide. *J. Catal.* **2015**, *331*, 162−171.
(29) Schweitzer, N. M.; Schaidle, J. A.; Ezekoye, O. K.; Pan, X.; Linic, S.; Thompson, L. T. High activity carbide supported catalysts for water gas shift. *J. Am. Chem. Soc.* **2011**, *133*, 2378−2381.
(30) Zhang, Q.; Tackett, B. M.; Wu, Q.; Chen, J. G. Trends in Hydrogen Evolution Activity of Metal-Modified Molybdenum Carbides in Alkaline and Acid Electrolytes. *ChemElectroChem* **2016**, *3*, 1686−1693.
(31) Frauwallner, M. L.; López-Linares, F.; Lara-Romero, J.; Scott, C. E.; Ali, V.; Hernández, E.; Pereira-Almao, P. Toluene hydrogenation at low temperature using a molybdenum carbide catalyst. *Appl. Catal., A* **2011**, *394*, 62−70.
(32) Mehdad, A.; Jentoft, R. E.; Jentoft, F. C. Passivation agents and conditions for Mo 2 C and W 2 C: Effect on catalytic activity for toluene hydrogenation. *J. Catal.* **2017**, *347*, 89−101.
(33) Sullivan, M. M.; Held, J. T.; Bhan, A. Structure and site evolution of molybdenum carbide catalysts upon exposure to oxygen. *J. Catal.* **2015**, *326*, 82−91.
(34) Lu, M.; Lu, F.; Zhu, J.; Li, M.; Zhu, J.; Shan, Y. Hydrodeoxygenation of methyl stearate as a model compound over Mo2C supported on mesoporous carbon. *React. Kinet., Mech. Catal.* **2015**, *115*, 251−262.
(35) Yang, T. T.; Saidi, W. A. Tuning the hydrogen evolution activity of β-Mo 2 C nanoparticles via control of their growth conditions. *Nanoscale* **2017**, *9*, 3252−3260.
(36) Chasvin, N.; Diez, A.; Pronsato, E.; Šedivá, R.; Johánek, V.; Volpe, M. A.; Pistonesi, C. Theoretical and experimental study of ethanol adsorption and dissociation on β-Mo 2 C surfaces. *Mol. Catal.* **2017**, *439*, 163−170.
(37) Liu, X.; Kunkel, C.; Ramírez de La Piscina, P.; Homs, N.; Viñes, F.; Illas, F. Effective and Highly Selective CO Generation from CO2 Using a Polycrystalline α-Mo2C Catalyst. *ACS Catal.* **2017**, *7*, 4323−4335.
(38) Kelly, T. G.; Hunt, S. T.; Esposito, D. V.; Chen, J. G. Monolayer palladium supported on molybdenum and tungsten carbide substrates as low-cost hydrogen evolution reaction (HER) electrocatalysts. *Int. J. Hydrogen Energy* **2013**, *38*, 5638−5644.
(39) Jäger, R.; Härk, E.; Romann, T.; Joost, U.; Lust, E. C(Mo2C) and Pt-C(Mo2C) based mixed catalysts for oxygen reduction reaction. *J. Electroanal. Chem.* **2016**, *761*, 89−97.
(40) Cao, J.; Ma, Y.; Guan, G.; Hao, X.; Ma, X.; Wang, Z.; Kusakabe, K.; Abudula, A. Reaction intermediate species during the steam

DOI: 10.1021/acsomega.7b01044
ACS Omega 2017, 2, 7976−7984

reforming of methanol over metal modified molybdenum carbide catalysts. *Appl. Catal., B* **2016**, *189*, 12−18.
(41) Saha, S.; Martin, B.; Leonard, B.; Li, D. Probing synergetic effects between platinum nanoparticles deposited via atomic layer deposition and a molybdenum carbide nanotube support through surface characterization and device performance. *J. Mater. Chem. A* **2016**, *4*, 9253−9265.
(42) Wang, X.; Perret, N.; Delannoy, L.; Louis, C.; Keane, M. A. Selective gas phase hydrogenation of nitroarenes over Mo ₂ C-supported Au-Pd. *Catal. Sci. Technol.* **2016**, *6*, 6932−6941.
(43) Tan, S.; Wang, L.; Saha, S.; Fushimi, R. R.; Li, D. Active Site and Electronic Structure Elucidation of Pt Nanoparticles Supported on Phase-Pure Molybdenum Carbide Nanotubes. *ACS Appl. Mater. Interfaces* **2017**, *9*, 9815−9822.
(44) Xiong, K.; Li, L.; Zhang, L.; Ding, W.; Peng, L.; Wang, Y.; Chen, S.; Tan, S.; Wei, Z. Ni-doped Mo2C nanowires supported on Ni foam as a binder-free electrode for enhancing the hydrogen evolution performance. *J. Mater. Chem. A* **2015**, *3*, 1863−1867.
(45) Zhang, X.; Zhu, X.; Lin, L.; Yao, S.; Zhang, M.; Liu, X.; Wang, X.; Li, Y.; Shi, C.; Ma, D. Highly dispersed Copper over β-Mo2C as Efficient and Stable Catalysts for RWGS Reaction. *ACS Catal.* **2017**, *7*, 912−918.
(46) Pistonesi, C.; Pronsato, M. E.; Bugyi, L.; Juan, A. The adsorption of CO on potassium doped molybdenum carbide surface: An ab-initio study. *Catal. Today* **2012**, *181*, 102−107.
(47) Hohenberg, P.; Kohn, W. *Phys. Rev.* **1964**, *136*, No. B864.
(48) Kohn, W.; Sham, L. J. Self-consistent equations including exchange and correlation effects. *Phys. Rev.* **1965**, *140*, No. A1133.
(49) Perdew, J. P.; Wang, Y. Accurate and simple analytic representation of the electron-gas correlation energy. *Phys. Rev. B: Condens. Matter Mater. Phys.* **1992**, *45*, No. 13244.
(50) Giannozzi, P.; Baroni, S.; Bonini, N.; Calandra, M.; Car, R.; Cavazzoni, C.; Ceresoli, D.; Chiarotti, G. L.; Cococcioni, M.; Dabo, I.; dal Corso, A.; de Gironcoli, S.; Fabris, S.; Fratesi, G.; Gebauer, R.; Gerstmann, U.; Gougoussis, C.; Anton, K.; Lazzeri, M.; Martin-Samos, L.; Marzari, N.; Mauri, F.; Mazzarello, R.; Paolini, S.; Pasquarello, A.; Paulotto, L.; Sbraccia, C.; Scandolo, S.; Sclauzero, G.; Seitsonen, A. P.; Smogunov, A.; Umari, P.; Wentzcovitch, R. M. QUANTUM ESPRESSO: a modular and open-source software project for quantum simulations of materials. *J. Phys.: Condens. Matter* **2009**, *21*, No. 395502.
(51) Kokalj, A. Computer graphics and graphical user interfaces as tools in simulations of matter at the atomic scale. *Comput. Mater. Sci.* **2003**, *28*, 155−168.
(52) *Jmol: An Open-source Java Viewer for Chemical Structures in 3D*. http://www.jmol.org/.
(53) Vanderbilt, D. Soft self-consistent pseudopotentials in a generalized eigenvalue formalism. *Phys. Rev. B* **1990**, *41*, No. 7892.
(54) Rudy, E.; Windisch, S.; Stosick, A.; Hoffman, J. Constitution of Binary Molybdenum-Carbon Alloys. *Trans. Metall. Soc. AIME* **1967**, *239*, 1247−67.
(55) Wentzcovitch, R. M. Invariant molecular-dynamics approach to structural phase transitions. *Phys. Rev. B* **1991**, *44*, No. 2358.
(56) Monkhorst, H. J.; Pack, J. D. Special points for Brillouin-zone integrations. *Phys. Rev. B* **1976**, *13*, No. 5188.
(57) Henkelman, G.; Uberuaga, B. P.; Jónsson, H. A climbing image nudged elastic band method for finding saddle points and minimum energy paths. *J. Chem. Phys.* **2000**, *113*, 9901−9904.
(58) Sanville, E.; Kenny, S.D.; Smith, R.; Henkelman, G. Improved grid-based algorithm for Bader charge allocation. *J. Comput. Chem.* **2007**, *28*, 899−908.
(59) Shi, Y.; Yang, Y.; Li, Y.-W.; Jiao, H. Activation mechanisms of H_2, O_2, H_2O, CO_2, CO, CH_4 and C_2H_x on metallic $Mo_2C(001)$ as well as Mo/C terminated $Mo_2C(101)$ from density functional theory computations. *Appl. Catal., A* **2016**, *524*, 223−236.
(60) Ren, J.; Huo, C.-F.; Wang, J.; Cao, Z.; Li, Y.-W.; Jiao, H. Density functional theory study into the adsorption of CO_2, H and CH_x (x = 0-3) as well as C_2H_4 on α-$Mo_2C(0001)$. *Surf. Sci.* **2006**, *600*, 2329−2337.
(61) Sensoy, M. G.; Toffoli, D.; Ustunel, H. Structural and electronic properties of bulk and low-index surfaces of zincblende PtC. *J. Phys.: Condens. Matter* **2017**, *29*, No. 125002.

DOI: 10.1021/acsomega.7b01044
ACS Omega 2017, 2, 7976−7984